JOURNAL OF COMPUTATIONAL PHYSICS 50, 235–269 (1983)

Self-Adjusting Grid Methods for One-Dimensional Hyperbolic Conservation Laws*

AMI HARTEN

School of Mathematical Sciences, Tel-Aviv University, Tel-Aviv, Israel

AND

JAMES M. HYMAN

Los Alamos National Laboratory, Los Alamos, New Mexico 87545

Received January 6, 1982; revised September 14, 1982

It is shown how to automatically adjust the grid to follow the dynamics of the numerical solution of hyperbolic conservation laws. The grid motion is determined by averaging the local characteristic velocities of the equations with respect to the amplitudes of the signals. The resulting algorithm is a simple extension of many currently popular Godunov-type methods. Computer codes using one of these methods can be easily modified to add the moving mesh as an option. Numerical examples are given that illustrate the improved accuracy of Godunov's and Roe's methods on a self-adjusting mesh.

I. INTRODUCTION

In this report we consider the initial value problem (IVP)

$$w_t + f(w)_x = 0; \qquad w(x, 0) = w_0(x), \qquad -\infty < x < \infty. \tag{1.1}$$

Here w is an m-column vector and the flux function $f(w)$ is a vector-valued function of m components. We assume that the Jacobian

$$A(w) = f_w(w) \tag{1.2a}$$

has m real eigenvalues

$$a_1(w) \leqslant a_2(w) \leqslant \cdots \leqslant a_m(w) \tag{1.2b}$$

and a complete set of right eigenvectors $\{R_k(w)\}_{k=1}^m$. Furthermore, we assume that the system of conservation laws has an entropy function. That is, a convex scalar

* Work supported by US Department of Energy, Office of Basic Energy Sciences, Department of Applied Mathematics under contract W-7405-ENG-36.

† Work partially supported by NASA-Ames Research Center, Moffett Field, Calif. under interchange number NCA2-OR-525-101 and by Tel-Aviv University, Tel-Aviv, Israel.

0021-9991/83 $3.00

function $U(w)$ and a corresponding entropy flux $F(w)$ exist such that all smooth solutions w of Eq. (1.1) satisfy

$$U(w)_t + F(w)_x = 0. \tag{1.3a}$$

On the other hand, physically relevant weak solutions of Eq. (1.1) satisfy the entropy inequality

$$U(w)_t + F(w)_x \leqslant 0 \tag{1.3b}$$

in the sense of distributions. Thus, admissible discontinuities in weak solutions of Eq. (1.1) satisfy the Rankine–Hugoniot (RH) condition

$$f(w_R) - f(w_L) = s(w_R - w_L) \tag{1.4a}$$

and the entropy jump inequality

$$F(w_R) - F(w_L) \leqslant S[U(w_R) - U(w_L)]. \tag{1.4b}$$

Here w_L and w_R are the states for the left and the right of the discontinuity and S is the speed of propagation of the discontinuity (see [10]).

We now discuss discrete approximations of weak solutions of IVP (1.1). Let $\{x_j\}$ be a fixed (not necessarily uniform) partition of the real line, and let $\{\xi^n_{j+1/2}\}$ be a variable partition of the real line that depends on the time level n. The set $\{I^n_j\}$ denotes the intervals defined by the partition $\{\xi^n_{j+1/2}\}$,

$$I^n_j = (\xi^n_{j-1/2}, \xi^n_{j+1/2}). \tag{1.5a}$$

We consider piecewise-constant approximations $v(x, t)$ to the solution $w(x, t)$ of Eq. (1.1), such that

$$v(x, t_n) = v^n_j, \qquad x \in I^n_j. \tag{1.5b}$$

A typical example of such a grid is shown in Fig. 1.

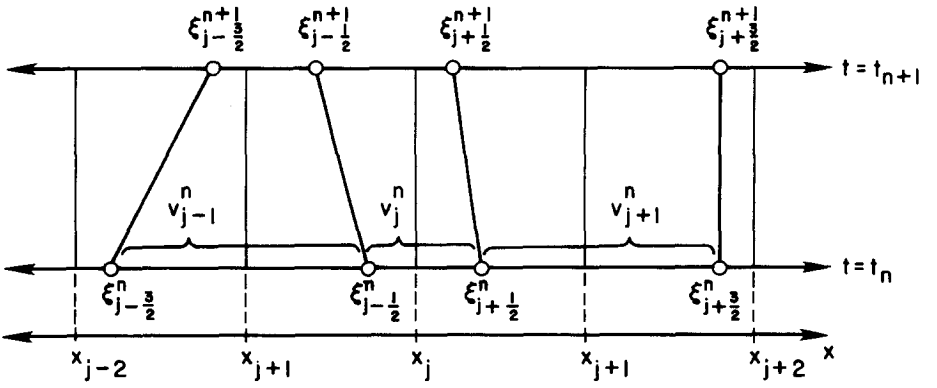

FIG. 1. The numerical methods are formulated in the trapezoidal regions.

We require that v_j^n approximate $w(x, t)$ in the following average sense:

Conservation form

$$(\xi_{j+1/2}^{n+1} - \xi_{j-1/2}^{n+1}) v_j^{n+1} = (\xi_{j+1/2}^{n} - \xi_{j-1/2}^{n}) v_j^{n} - \tau^n (\bar{f}_{j+1/2} - \bar{f}_{j-1/2}); \tag{1.6a}$$

Entropy inequality

$$(\xi_{j+1/2}^{n+1} - \xi_{j-1/2}^{n+1})\, U(v_j^{n+1}) \leqslant (\xi_{j+1/2}^{n} - \xi_{j-1/2}^{n})\, U(v_j^{n}) - \tau^n (\bar{F}_{j+1/2} - \bar{F}_{j+1/2}). \tag{1.6b}$$

Here $\tau^n = t_{n+1} - t_n$ and $\bar{f}_{i+1/2}$ and $\bar{F}_{i+1/2}$ are numerical fluxes consistent with the fluxes of Eqs. (1.1) and (1.3) through the line connecting $\xi_{i+1/2}^n$ and $\xi_{i+1/2}^{n+1}$, in the $x - t$ plane, respectively.

Schemes in conservation form on a fixed mesh, where $\xi_{j+1/2}^n \equiv \xi_{j+1/2}$ for all n, cannot in general resolve shocks as perfect discontinuities. When the shock location is in the interior of the interval I_j^n, conservation requirement (1.6a) implies that v_j^n is an average of w_L and w_R. Thus a certain amount of smearing is inherent in fixed mesh calculations in conservation form.

Smearing admissible discontinuities in a fixed mesh calculation can be avoided by using a random choice method [2] or by a shock-fitting approach [11]. In the random choice method, the strict conservation (1.6a) is replaced by a requirement of conservation in the mean. When a shock location is in the interior of an interval I_j^n, then v_j^n is chosen randomly to be either w_L or w_R, thus keeping the discontinuity sharp. The sampling of the two states is such that the expected value of the propagation speed of the shock satisfies RH condition (1.4a) [6].

In the shock-fitting approach the discontinuity is considered a moving internal boundary, the motion of which is determined by w_L, w_R, and the RH condition. Once the shock location at the advanced time level is known, w_L^{n+1}, w_R^{n+1}, and v_j^{n+1} are computed as two coupled boundary value problems.

Another technique to achieve perfect resolution of a particular discontinuity is front tracking. As in shock fitting, propagation of the shock front is followed explicitly; unlike shock fitting, the shock front is not considered a moving internal boundary. The perfect resolution of the shock is obtained by making its location coincide with a mesh point, say ξ_j^n, and by using a numerical scheme that can perfectly resolve a stationary shock. When applied to a self-adjusting mesh calculation in which ξ_j^n lies on the path of the shock for all n, the numerical flux $\bar{f}_j^n$, when considered in a system of coordinates that moves with the speed of the shock $(\xi_j^{n+1} - \xi_j^n)/\tau^n$, is identical to that corresponding to a stationary shock, thus yielding a perfect resolution [8, 9].

In this report, we consider numerical solutions using deterministic schemes in conservation form on a self-adjusting grid. The interval end points $\{\xi_{j+1/2}^n\}$ are constrained to satisfy

$$x_j < \xi_{j+1/2}^n \leqslant x_{j+1}, \tag{1.7}$$

where x_j is the underlying fixed mesh. The location of the discontinuities $\xi_{j+1/2}^n$ is considered a variable associated with the $(x_j, x_{j+1}]$ cell of the fixed mesh.

Unlike front tracking, we adopt the point of view of Godunov [3] and consider each discontinuity of $v(x, t_n)$ at $\{\xi^n_{j+1/2}\}$ a Riemann problem. We select $\xi^{n+1}_{j-1/2}$ at the advanced time level in such a way that the averaging procedure used to define v^{n+1}_j in $(\xi^{n+1}_{j-1/2}, \xi^{n+1}_{j+1/2})$ will retain information about the most significant waves in the neighboring Riemann problems. In particular, if a single shock or a contact discontinuity is the solution of the Riemann problem at $\xi^n_{i+1/2}$, the mesh algorithm automatically places one of the mesh points $\{\xi^{n+1}_{i-1/2}, \xi^{n+1}_{i+1/2}, \xi^{n+1}_{i+3/2}\}$ on the path of this discontinuity, thus enabling its perfect resolution.

The goal of this preliminary study is to investigate the effect of a self-adjusting mesh on the quality of numerical approximations obtained by Godunov-type schemes. We stress the improvement in the methods caused by the self-adjusting mesh algorithm, rather than the relative performance of various schemes.

In Section II we describe Godunov-type schemes on a moving grid and in particular derive an expression for the numerical fluxes of the Godunov scheme [3] and the Roe scheme [12]. In Section III we describe a self-adjusting mesh algorithm that minimizes the diffusion in Godunov-type schemes, and in Section IV we present some numerical experiments that illustrate certain features of numerical solutions of Godunov's scheme and of Roe's scheme on the proposed self-adjusting grid. In the Appendices we derive a version of Roe's scheme that satisfies the entropy inequality.

II. Godunov-Type Schemes on a Variable Mesh

In this section we construct Godunov-type schemes on a variable mesh. Consider the IVP

$$w_t + f(w)_x = 0, \qquad w(x, 0) = v(x, t_n), \qquad -\infty < x < \infty, \tag{2.1a}$$

where $v(x, t_n)$ is the piecewise-constant approximation (1.5) to the solution of Eq. (1.1) at $t = t_n$. Next we obtain an approximation $w^n(x, t)$ to the solution of (2.1a) for $0 \leqslant t \leqslant \tau$, $-\infty < x < \infty$, when τ is sufficiently small. Once we have evaluated $w^n(x, \tau)$, we define the new piecewise-constant approximation $v(x, t_{n+1})$ by

$$v^{n+1}_j = \frac{1}{\xi^{n+1}_{j+1/2} - \xi^{n+1}_{j-1/2}} \int_{I^{n+1}_j} w^n(x, \tau)\, dx \tag{2.1b}$$

and

$$v(x, t_{n+1}) = v^{n+1}_j, \qquad x \in I^{n+1}_j. \tag{2.1c}$$

We construct $w^n(x, t)$ from approximate solutions to the Riemann problems for the jump discontinuities in $v(x, t_n)$ at the points $\{\xi^n_{j+1/2}\}$. The solution to the Riemann problem

$$\begin{aligned} w_t + f(w)_x = 0, \qquad w(x, 0) &= W_L, \qquad x < 0, \\ &= W_R, \qquad x > 0, \end{aligned} \tag{2.2}$$

is self-similar in the variable x/t; therefore, we consider self-similar approximate solutions to Eq. (2.2), which we denote by $w(x/t;\ w_L, w_R)$. Because of the hyperbolic nature of the system of conservation laws, there is a finite domain of influence of the discontinuity at $x = 0$. We assume that same for the approximate solution $w(x/t;\ w_L, w_R)$; that is, there exist finite speeds $a^L = a^L(w_L, w_R)$ and $a^R = a^R(w_L, w_R)$, where

$$-\infty < a^L \leqslant a^R < +\infty \tag{2.3}$$

and $w(x/t;\ w_L, w_R) = w_L$, for $x/t < a^L$ and $w(x/t;\ w_L, w_R) = w_R$ when $x/t > a^R$.

We now consider the approximate solution to the Riemann problem $w(x/t;\ v_j^n, v_{j+1}^n)$ and denote by the subscript $j + \frac{1}{2}$ quantities associated with it. To assure no interaction between the two neighboring Riemann problems at $j - \frac{1}{2}$ and $j + \frac{1}{2}$, we restrict the time step τ by the Courant–Friedrichs–Lewy (CFL)-like time-step restrictions

$$\xi_{j-1/2}^n + a_{j-1/2}^R \tau \leqslant \tfrac{1}{2}(\xi_{j-1/2}^n + \xi_{j+1/2}^n)$$

and

$$\xi_{j+1/2}^n + a_{j+1/2}^L = \tfrac{1}{2}(\xi_{j-1/2}^n + \xi_{j+1/2}^n).$$

Hence for $0 \leqslant t \leqslant \tau$, where

$$\tau \max_j \{a_{j-1/2}^R/(\xi_{j+1/2}^n - \xi_{j-1/2}^n), -a_{j+1/2}^L/(\xi_{j+1/2}^n - \xi_{j-1/2}^n)\} \leqslant \tfrac{1}{2}, \tag{2.4}$$

the function $w^n(x, t)$ defined by

$$w^n(x, t) = w[(x - \xi_{j+1/2}^n)/t;\ v_j^n, v_{j+1}^n] \tag{2.5}$$

for

$$\tfrac{1}{2}(\xi_{j-1/2}^n + \xi_{j+1/2}^n) \leqslant x \leqslant \tfrac{1}{2}(\xi_{j+1/2}^n + \xi_{j+3/2}^n)$$

is univalued. Thus a Godunov-type scheme corresponding to the approximate solution of the Riemann problem $w(t/t;\ w_L, w_R)$ can be formally defined by Eqs. (2.1), (2.4), and (2.5). However, to make the resulting Godunov-type scheme a meaningful approximation to physically relevant weak solutions of Eq. (1.1), more properties of $w(x/t;\ w_L, w_R)$ are needed.

In [7, Theorem 2.1], Harten and Lax assert that if $w(x/t;\ w_L, w_R)$ is a Lipschitz continuous function

$$|w(x/t;\ w_L, w_R)| \leqslant O(|w_R - w_L|) \tag{2.6a}$$

that satisfies the following conditions:

consistency with the integral form of the conservation law

$$\int_{-\Delta}^{\Delta} w(x/\tau; w_L, w_R)\,dx = \Delta(w_L + w_R) - \tau[f(w_R) - f(w_L)], \tag{2.6b}$$

consistency with the integral form of entropy inequality (1.3b)

$$\int_{-\Delta}^{\Delta} U(w(x/\tau; w_L, w_R))\,dx \leqslant \Delta[U(w_L) + U(w_R)] - \tau[F(w_R) - F(w_L)] \tag{2.6c}$$

for all t and Δ such that

$$-\Delta \leqslant \tau a^L \leqslant \tau a^R \leqslant +\Delta, \tag{2.6d}$$

then a Godunov-type scheme defined by Eqs. (2.1) and (2.5) under time step restriction (2.4) has conservation form (1.6a) and satisfies entropy inequality (1.6b).

This entropy inequality implies that the numerical solution is bounded in the l_2 norm [8]. However, l_2 stability does not imply convergence in the nonlinear case.

Consistency relation (2.6b) enables us to define a numerical flux function $\bar{f}(\dot{\xi}; w_L, w_R)$ that approximates the flux of Eq. (1.1) through the line $\dot{\xi} = x/t$ as seen in Fig. 2 by the relation

$$\tau\bar{f}(\dot{\xi}; w_L, w_R) = \tau f(w_L) + \Delta w_L - \int_{-\Delta}^{\dot{\xi}\tau} w(x/\tau; w_L, w_R)\,dx \tag{2.7a}$$

or, after rearranging,

$$\int_{-\Delta}^{\dot{\xi}\tau} w(w/\tau; w_L, w_R)\,dx = \Delta w_L - \tau[\bar{f}(\dot{\xi}; w_L, w_R) - f(w_L)]. \tag{2.7b}$$

To see that Lipschitz continuity assumption (2.6a) implies that $w(x/t; v, v) \equiv v$; consequently, (note that the numerical flux $\bar{f}(\dot{\xi}; w_L, w_R)$ is consistent with the flux of Eq. (1.1) through any line $x/t = \dot{\xi}$):

$$\begin{aligned}\tau\bar{f}(\dot{\xi}; v, v) &= \tau f(v) - \Delta v - \int_{-\Delta}^{\dot{\xi}\tau} w(x/\tau; v, v)\,dx \\ &= \tau f(v) - \Delta v - (v\tau + \Delta)v = \tau[f(v) - \dot{\xi}v].\end{aligned} \tag{2.8}$$

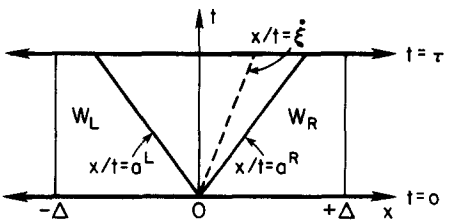

FIG. 2. The flux through the line $\dot{\xi} = x/t$ is approximated in Eq. (2.8).

Hence,

$$\bar{f}(\dot{\xi}; v, v) = f(v) - \dot{\xi}v$$

for all $\dot{\xi}$ and v.

Having obtained a numerical flux function $\bar{f}(\dot{\xi}; w_L, w_R)$, we may now define the corresponding conservation form scheme on a variable mesh by

$$(\xi^{n+1}_{j+1/2} - \xi^{n+1}_{j-1/2})v^{n+1}_j = (\xi^n_{j+1/2} - \xi^n_{j-1/2})v^n_j - \tau\{\bar{f}[(\xi^{n+1}_{j+1/2} - \xi^n_{j+1/2})/\tau; v^n_j, v^n_{j+1}] - \bar{f}[(\xi^{n+1}_{j-1/2} - \xi^n_{j-1/2})/\tau; v^n_{j-1}, v^n_j]\}. \tag{2.9}$$

A typical example of such a mesh is shown in Fig. 1.

The conservation form scheme (2.7) and (2.9) is well defined for all $\{\xi^n_{j+1/2}\}$ and τ. However, it becomes identical with Godunov-type scheme (2.1) and (2.5) only if τ is restricted by Eq. (2.4) and if $\xi^n_{j+1/2}$ is an increasing function of j.

The CFL-like time-step restriction (2.4) is used to represent the Godunov-type scheme (2.1) and (2.5) as a univalued average of approximate solutions to local Riemann problems; it is also used in the Harten–Lax theorem in proving the entropy inequality. In the constant coefficient case, this less stringent condition can be proven to be sufficient for stability and has been found numerically to be sufficient for the scheme to be stable in the nonconstant coefficient case.

In the methods presented here we require that the domain of influence of the Riemann problem at $\xi^n_{j+1/2}$ be contained at $t = t_{n+1}$ in $(\xi^{n+1}_{j-1/2}, \xi^{n+1}_{j+3/2})$; that is,

$$\xi^{n+1}_{j-1/2} \leqslant \xi^n_{j+1/2} + a^L_{j+1/2}\tau \leqslant \xi^n_{j+1/2} + a^R_{j+1/2}\tau \leqslant \xi^{n+1}_{j+3/2}, \tag{2.10a}$$

which allows a time step twice as large as Eq. (2.4); that is,

$$\tau \max_j \{a^R_{j-1/2}/(\xi^n_{j+1/2} - \xi^n_{j-1/2}), -a^L_{j+1/2}/(\xi^n_{j+1/2} - \xi^n_{j-1/2})\} \leqslant 1. \tag{2.10b}$$

We now describe two versions of Godunov-type schemes.

A. *Godunov's Method*

In Godunov's scheme [3], the exact solution to Riemann problem (2.2) is used. Of course the exact solution satisfies all requirements (2.6) of the Harten–Lax theorem; consequently, scheme (2.1) and (2.5) has conservation form (2.9) and satisfies entropy inequality (1.6b). Because $w(x/t; w_L, w_R)$ satisfies the differential equation in the domain $-\Delta \leqslant x \leqslant \dot{\xi}\tau$ when $t \leqslant \tau$,

$$\int_0^\tau dt \int_{-\Delta}^{\dot{\xi}\tau} dx[w_t + f(w)_x] = 0. \tag{2.11a}$$

Using this to evaluate numerical flux (2.7b) we have

$$\bar{f}(v; w_L, w_R) = f(w(v; w_L w_R)) - \dot{\xi}w(v; w_L, w_R). \tag{2.11b}$$

An algorithm for computation of the exact solution of the Riemann problem for the Euler equations has been developed by Godunov and modified by Chorin [2]. This algorithm takes a simple form because the second wave for the Euler equations of gas dynamics can be only a contact discontinuity. However, when measured relative to the computer execution time of a flux computation, it is still an expensive algorithm.

B. *Roe's Method*

In Roe's scheme [13], a linearized equation is used to approximate the solution to the Riemann problem. Roe constructs a constant mean value Jacobian $A(w_L, w_R)$, such that

$$f(w_R) - f(w_L) = A(w_L, w_R)(w_R - w_L), \tag{2.12a}$$

and $A(w_L, w_R)$ is consistent with the Jacobian, $A(w, w) = f_w(w)$, and has real eigenvalues

$$a_1(w_L, w_R) \leqslant a_1(w_L, w_R) \leqslant \cdots \leqslant a_m(w_L, w_R)$$

and a complete system of right eigenvectors $\{R_k(w_L, w_R)\}_{k=1}^m$, for all w_L and w_R.

The approximate solution $w(x/t; w_L, w_R)$ is taken to be the solution of the constant coefficient linear Riemann problem

$$w_t + A(w_L, w_R) w_x = 0, \tag{2.12b}$$

with the initial conditions

$$\begin{aligned} w(x, 0) &= w_L, \qquad x < 0, \\ &= w_R, \qquad x > 0. \end{aligned}$$

Substituting this solution for $w(x/t; w_L, w_R)$ in Eq. (2.7b), we obtain

$$\bar{f}(\dot{\xi}; w_L, w_R) = \tfrac{1}{2}\left[\bar{f}(w_L) + \bar{f}(w_R) - \sum_{k=1}^{m} \alpha_k |\bar{a}_k| R_k(w_L, w_R)\right], \tag{2.13a}$$

where the $\alpha_k(w_L, w_R)$ are defined by the relation

$$w_R - w_L = \sum_{k=1}^{m} \alpha_k R_k(w_L, w_R), \tag{2.13b}$$

and $\bar{f}(w)$ and $\bar{a}_k(w_L, w_R)$ are

$$\bar{f}(w) = f(w) - \dot{\xi} w \tag{2.13c}$$

and

$$\bar{a}_k(w_L, w_R) = a_k(w_L, w_R) - \dot{\xi}. \tag{2.13d}$$

Roe's scheme (2.9) and (2.13) is in conservation form and is monotonicity preserving in the characteristic variables for the constant coefficient case; however, it may violate entropy inequality (1.6b) (see [8]).

To prevent entropy violation we modify Roe's scheme by adding an entropy viscosity term as described in Appendix A. The effect is to replace the quantity $|\bar{a}_k|$ in (2.13a) by $Q_k(\bar{a}_k)$, where

$$\begin{aligned} Q_k(x) &= |x|, \qquad |x| \geqslant \delta_k, \\ &= \delta_k, \qquad |x| < \delta_k, \end{aligned} \tag{2.14a}$$

i.e.,

$$\bar{f}(\xi; w_L, w_R) = \tfrac{1}{2}\left[\bar{f}(w_L) + \bar{f}(w_R) - \sum_{k=1}^{m} \alpha_R Q_R(\bar{a}_R) R_R(w_L, w_R)\right]. \tag{2.14b}$$

Here, $\delta_k = \delta_k(w_L, w_R)$ is a nonnegative quantity that measures the violation of the entropy condition in the kth characteristic field; $\delta_k = 0$ if and only if the kth wave in the solution to (2.12b) is a shock. See the Appendix for more details.

Roe's scheme even as modified in (2.14), in our opinion, is considerably simpler and computationally more efficient than Godunov's scheme. In this report we will use this modified Roe scheme unless otherwise stated. In [12] additional ways to use the linearization are presented.

III. A Self-Adjusting Mesh Algorithm

In this section we describe a self-adjusting mesh for computations with Godunov-type schemes. The approximation associated with those first-order accurate Godunov-type schemes of Section II is that of piecewise-constant functions; that is,

$$v(x, t_n) = v_j^n \qquad \text{for} \quad \xi_{j-1/2}^n < x \leqslant \xi_{j+1/2}^n. \tag{3.1}$$

We consider the case where the interval end points $\{\xi_{j+1/2}^n\}$ are constrained by

$$x_j < \xi_{j+1/2}^n \leqslant x_{j+1} \tag{3.2}$$

for all j and n. Here x_j is an underlying fixed grid (not necessarily uniform). Thus $\{\xi_{j+1/2}^n\}$ is a variable associated with the $(x_j, x_{j+1}]$ cell of the underlying fixed mesh (see Fig. 2).

Given $\{\xi_{j+1/2}^0\}$ and $\{v_j^0\}$, we construct a self-adjusting mesh algorithm that selects $\{\xi_{j+1/2}^{n+1}\}$, $n \geqslant 0$ to satisfy the following requirements:

(1) v_j^{n+1} computed by a Godunov-type scheme (2.1) and (2.5) should capture the main features of the neighboring Riemann problems at $j \pm 1/2$; in particular, if at time t_n a single isolated admissible discontinuity emerges from a neighboring Riemann problem and ends at time t_{n+1} in the half-open set $(x_j, x_{j+1}]$, then $\xi_{j+1/2}^{n+1}$ should coincide with its location.

(2) $\xi_{j+1/2}^{n+1}$ is an increasing univalued function of the cells $(x_j, x_{j+1}]$. This implies there is exactly one interval end point in each cell $(x_j, x_{j+1}]$.

(3) If $\xi_{j+1/2}^0 - \xi_{j-1/2}^0 \geqslant \frac{1}{2}d_j$, then

$$\xi_{j+1/2}^{n+1} - \xi_{j-1/2}^{n+1} \geqslant \tfrac{1}{2}d_j \qquad \text{for all } j \text{ and } n, \tag{3.3a}$$

where

$$d_j = \min\{x_{j+1} - x_j, x_j - x_{j-1}\}. \tag{3.3b}$$

The last requirement (3.3) ensures that the time step τ^n in Eq. (2.10b) is bounded away from zero. The most stringent condition in Eq. (2.10b) is then

$$\tau^n \max_j\{a_{j-1/2}^{\mathrm{R}}/d_j, -a_{j-1/2}^{\mathrm{L}}/d_j\} \leqslant \tfrac{1}{2}. \tag{3.4}$$

This corresponds to limiting the CFL number of $\frac{1}{2}$ with respect to the corresponding CFL condition on the fixed underlying grid.

The solution $w(x/t;\ w_{\mathrm{L}}, w_{\mathrm{R}})$ to Riemann problem (2.2) is a fan of m-waves arranged in increasing order in the index of the characteristic fields (1.2b). If the kth characteristic field is genuinely nonlinear, then the k-wave is a shock or a rarefaction, depending on whether the kth field is convergent or divergent, respectively. When the kth characteristic field is linearly degenerate, the k-wave is a contact discontinuity (see [10]). Figure 3 illustrates how these waves propogate in two neighboring Riemann problems.

The numerical solution v_j^{n+1} is computed as the average (2.1b) of the part of the solutions to the Riemann problem at $x = \xi_{j-1/2}^n$ and $x = \xi_{j+1/2}^n$, which is contained in the interval $I_j^{n+1} = (\xi_{j-1/2}^{n+1}, \xi_{j+1/2}^{n+1}]$. Consequently, the smearing caused by averaging of a k-wave in the $j + \frac{1}{2}$ Riemann problem depends on its distance from $\xi_{j+1/2}^{n+1}$. Maximal diffusion in a k-wave occurs when it falls in the center of the interval I_j^{n+1}

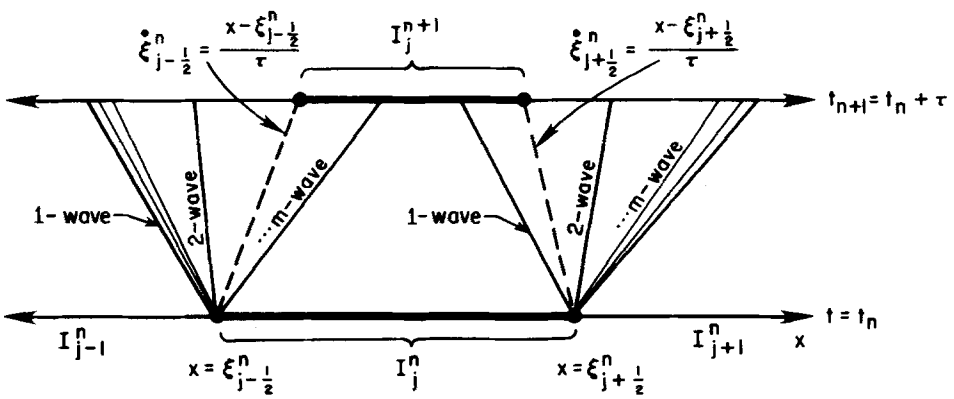

FIG. 3. The solutions to the Riemann problems at $\xi_{j\pm1/2}$ are composed of constant states separated by a fan a characteristic lines.

or I_{j+1}^{n+1}; minimal smearing occurs when the wave falls on an end point of the interval.

Unfortunately, there is one interval end point per m-wave; therefore we cannot prevent diffusion of all m-waves for $m > 1$ by selection of a single point $\xi_{j+1/2}^{n+1}$. Consequently, we compromise and choose interval end points that minimize, in a certain sense, the overall diffusion in the Godunov-type scheme. We do so by moving the interval end points with a speed $\dot{\xi}(w_L, w_R)$, which is a weighted average of the m speeds of propagation of the waves in $w(x/\tau; w_L, w_R)$ such that

$$a^L(w_L, w_R) \leqslant \dot{\xi}(w_L, w_R) \leqslant a^R(w_L, w_R); \tag{3.5a}$$

see Eq. (2.3) and Fig. 2.

We consider $\dot{\xi}(w_L, w_R)$, where the weight assigned to the kth characteristic speed represents the relative significance of the k-wave in the Riemann problem. We shall use weights that are monotone increasing functions of the amplitude of the wave that vanish if and only if the magnitude of the wave is zero. It follows from this property that if $w(x/t; w_L, w_R)$ is a single shock or a contact discontinuity moving with a speed s_k, then

$$\dot{\xi}(w_L, w_R) = s_k. \tag{3.5b}$$

We see now that we can satisfy requirement (1) of this section by moving the interval end points $\xi_{j+1/2}^n$ with the speed $\dot{\xi}_{j+1/2}^n = \dot{\xi}(v_j^n, v_{j+1}^n)$. However, this strategy may violate requirement (2), because it is possible to have none or more than one interval end point in the cell $(x_j, x_{j+1}]$ at $t = t_{n+1}$. We therefore consider such motion of the grid to provide temporary values $\{\bar{\xi}_{j+1/2}^{n+1}\}$ for the interval end points

$$\bar{\xi}_{j+1/2}^{n+1} = \xi_{j+1/2}^n + \tau^n \dot{\xi}_{j+1/2}^n. \tag{3.6}$$

Under time-step restriction (2.10), inequality (3.5a) implies that $\{\bar{\xi}_{j+1/2}^{n+1}\}$ either stays in the cell $(x_j, x_{j+1}]$ or lands in one of the immediate neighboring cells $(x_{j-1}, x_j]$ or $(x_{j+1}, x_{j+2}]$. Thus, at time t_{n+1}, the cell $(x_j, x_{j+1}]$ may contain any of $\{\bar{\xi}_{j-1/2}^{n+1}, \bar{\xi}_{j+1/2}^{n+1}, \bar{\xi}_{j+3/2}^{n+1}\}$, or none.

To satisfy requirement (2) we use the following strategy: if one or more of the above mentioned points $\{\bar{\xi}_{j-1/2}^{n+1}\}$ is in the cell $(x_j, x_{j+1}]$, we assign a single location $\hat{\xi}_{j-1/2}^{n+1}$, which is a weighted average of the location of the points in the cell; the weights are proportional to the amplitude of the Riemann problem associated with the moving interval end point. If there is no point of $\{\bar{\xi}^{n+1}\}$ in $(x_j, x_{j+1}]$, we assign $\hat{\xi}_{j+1/2}^{n+1}$ to the center of the cell.

We accomplish all this in a single sweep over the mesh, defining

$$\hat{\xi}_{j+1/2}^{n+1} = \tfrac{1}{2}(x_j + x_{j+1}) + \left\{ \sum_{l=-1}^{1} [\bar{\xi}_{j+l+1/2} - \tfrac{1}{2}(x_j + x_{j+1})] \right.$$

$$\left. \times \bar{\beta}_{j+l+1/2} h(\bar{\xi}_{j+l+1/2}; x_j, x_{j+1}) \right\} \Big/ \hat{\beta}_{j+1/2}. \tag{3.7a}$$

Here $\bar{\beta}_{i+1/2} = \bar{\beta}(v_i^n, v_{i+1}^n)$ is a weight representing the magnitude of the Riemann problem associated with $\bar{\xi}_{i+1/2}^{n+1}$, and $h(x; a, b)$ is the interval function of (a, b),

$$h(x; a, b) = \tfrac{1}{2}[\operatorname{sgn}(x-a) + \operatorname{sgn}(b-x)]. \tag{3.7b}$$

That is, $h = 1$ for $a < x \leqslant b$, and $h = 0$ otherwise: $\hat{\beta}_{j+1/2}$ is a weighted amplitude of the waves present in the cell $(x_j, x_{j+1}]$ at $t = t_{n+1}$,

$$\hat{\beta}_{j+1/2} = \sum_{l=-1}^{1} \bar{\beta}_{j+l+1/2} h(\bar{\xi}_{j+l+1/2}; x_j, x_{j+1}) + \varepsilon. \tag{3.7c}$$

Here ε is a relative cutoff value that is at least one order larger than the round-off error on the computing machine used. (From now on we use this cutoff convention for all nonnegative denominators.)

We note that if one of the interval end points $\{\bar{\xi}_{j-1/2}^{n+1}, \bar{\xi}_{j+1/2}^{n+1}, \bar{\xi}_{j+3/2}^{n+1}\}$ corresponds to a single isolated admissible discontinuity propagating from one constant state into another, then $\hat{\xi}_{j+1/2}^{n+1}$ in (3.7) coincides with its location.

After calculating $(\hat{\xi}_{j+1/2}^{n+1})$ by Eq. (3.7) we have exactly one interval mesh point in each cell $(x_j, x_{j+1}]$; however, $\hat{\xi}_{j-1/2}^{n+1}$ and $\hat{\xi}_{j+1/2}^{n+1}$ may both come very close to x_j, thus violating requirement (3). The last stage of our self-adjusting mesh algorithm is a regularization step that enforces requirement (3). In this step we examine the length of each interval $\hat{I}_j^{n+1} = (\hat{\xi}_{j-1/2}^{n+1}, \hat{\xi}_{j+1/2}^{n+1}]$. If the length of the $\hat{I}_j^{n+1}$ interval is larger than $\frac{1}{2}d_j$ in (3.3b), we leave it unchanged. If its length is smaller than $\frac{1}{2}d_j$, we push its end points apart until its length becomes exactly $\frac{1}{2}d_j$, by

$$\xi_{j-1/2}^{n+1} = \hat{\xi}_{j-1/2}^{n+1} - \tfrac{1}{2}d_j\hat{\beta}_{j+1/2}/(\hat{\beta}_{j+1/2} + \hat{\beta}_{j-1/2}) \tag{3.8a}$$

and

$$\xi_{j+1/2}^{n+1} = \hat{\xi}_{j+1/2}^{n+1} + \tfrac{1}{2}d_j\hat{\beta}_{j-1/2}/(\hat{\beta}_{j+1/2} + \hat{\beta}_{j-1/2}), \tag{3.8b}$$

where $\hat{\beta}_{j+1/2}$ is defined by Eq. (3.7c). It is easy to see that $\{\xi_{j+1/2}^{n+1}\}$, the results of this operation, satisfy requirements (1)–(3). In particular, if there is an isolated admissible discontinuity propagating from one constant state into another, its location at t_{n+1} coincides with one of the interval end points.

We now complete the description of the self-adjusting mesh algorithm (3.6)–(3.8) by specifying expressions for $\dot{\xi}(w_L, w_R)$ in Eq. (3.6) and $\bar{\beta}(w_L, w_R)$ in Eq. (3.7a).

First we describe such expressions that are convenient for computations with Roe's scheme (2.13) or (2.14).

We define

$$\bar{\beta}(w_L, w_R) = \sum_{k=1}^{m} [\alpha_k(w_L, w_R)]^2 \tag{3.9a}$$

and

$$\dot{\xi}(w_L, w_R) = \sum_{k=1}^{m} \alpha_k^2 a_k(w_L, w_R)/\bar{\beta}(w_L, w_R), \tag{3.9b}$$

where $a_k(w_L, w_R)$ are the eigenvalues of the mean value Jacobian $A(w_L, w_R)$ in Eq. (2.12), and $\alpha_k(w_L, w_R)$ are given by Eq. (2.13b). The jump in the kth characteristic variable in the linearized Riemann problem (2.12b) is $\alpha_k(w_L, w_R)$ and is therefore an approximation to the amplitude of the k-wave. Relation (2.12a) implies that if w_L and w_R satisfy the RH condition (1.4a), then

$$S(w_R - w_L) = f(w_R) - f(w_L) = A(w_L, w_R)(w_R - w_L).$$

Thus $w_R - w_L$ is a right eigenvector of $A(w_L, w_R)$ and $a_k(w_L, w_R)$ is a characteristic speed. It follows from Eq. (2.13b) that $\alpha_j(w_L, w_R) = 0$ for $j \neq k$, and therefore in Eq. (3.9b), $\dot{\xi}(w_L, w_R) = S = a_k$.

Note that α_k and a_k, needed to evaluate Eq. (3.9), are also needed to compute the numerical flux (2.13)–(2.14) of Roe's scheme. Thus the self-adjusting mesh algorithm requires only a little extra computer execution time.

Next we consider the following expressions for $\bar{\beta}(w_L, w_R)$ in Eq. (3.7a) and $\dot{\xi}(w_L, w_R)$ in Eq. (3.6) convenient for Godunov's method:

$$\bar{\beta}(w_L, w_R) = (w_R - w_L) \cdot [U_w(w_R) - U_w(w_L)] \tag{3.10a}$$

and

$$\dot{\xi}(w_L, w_R) = [f(w_R) - f(w_L)] \cdot [U_w(w_R) - U_w(w_L)]/\bar{\beta}(w_L, w_R). \tag{3.10b}$$

Here U_w is the gradient of the entropy function and $\cdot$ denotes the Euclidean inner product. Although Eq. (3.10) does not contain explicit evaluation of α_k and a_k, it is identical with Eq. (3.9) for a particular choice of a mean value Jacobian $A(w_L, w_R)$. To show this, we follow the results of Harten [4] and use a succession of mean-value procedures:

$$U_w(w_R) - U_w(w_L) = P(w_L, w_R)(w_R - w_L) \tag{3.11a}$$

and

$$f(w_R) - f(w_L) = S(w_L, w_R)[U_w(w_R) - U_w(w_L)] \tag{3.11b}$$

to get

$$f(w_R) - f(w_L) = SP(w_R - w_L). \tag{3.11c}$$

Here P is a positive definite matrix such that $P(w, w) = U_{ww} > 0$ and S is a symmetric matrix such that

$$S(w, w) = \partial f/\partial U_w.$$

Relation (3.11c) is the same as Eq. (2.12a) with $A(w_L, w_R) = SP$. Next we rewrite Eq. (3.10) as

$$\bar{\beta}(w_L, w_R) = (w_R - w_L) \cdot P(w_R - w_L) = \|P^{1/2}(w_R - w_L)\|^2 \tag{3.12a}$$

and

$$\dot{\xi}(w_L, w_R) = [SP(w_R - w_L)] \cdot [P(w_R - w_L)]/\bar{\beta}(w_L, w_R)$$
$$= [(P^{1/2}SP^{1/2})\, P^{1/2}(w_R - w_L)] \cdot [P^{1/2}(w_R - w_L)]/\bar{\beta}(w_L, w_R). \quad (3.12b)$$

The matrix $P^{1/2}SP^{1/2} = P^{1/2}A(w_L, w_R)P^{-1/2}$ is symmetric and similar to $A(w_L, w_R)$.

Let $\{E_k\}$ be the orthonormal system of eigenvectors of $P^{1/2}SP^{1/2}$ and $\tilde{\alpha}_k$ be the coefficients in the representation

$$P^{1/2}(w_R - w_L) = \sum_{k=1}^{m} \tilde{\alpha}_k E_k.$$

Then Eq. (3.9) becomes

$$\bar{\beta}(w_L, w_R) = \sum_{k=1}^{m} \tilde{\alpha}_k^2 \quad (3.13a)$$

and

$$\dot{\xi}(w_L, w_R) = \sum_{k=1}^{m} \tilde{\alpha}_k^2 a_k/\bar{\beta}(w_L, w_R), \quad (3.13b)$$

where a_k are the eigenvalues of $A(w_L, w_R) = SP$. However, R_k, the right eigenvectors of $A(w_L, w_R)$, are related by $R_k = P^{-1/2}E_k$ to the eigenvectors E_k of $P^{1/2}SP^{1/2}$; therefore Eq. (3.13) and consequently Eq. (3.10) are identical with Eq. (3.9) for this particular $A(w_L, w_R)$.

IV. Numerical Examples

The numerical methods described thus far have been for general systems of hyperbolic conservation laws. The numerical examples will be for the simple but important case—the Euler equations for an inviscid compressible polytropic gas. These equations can be written in the form of Eq. (1.1) with

$$w = (\rho, m, E)^T, \qquad f(w) = uw + (0, p, pu)^T, \quad (4.1)$$

where ρ = mass density, u = the velocity, $m = \rho u$ is the momentum, E = the total energy per unit volume, and $p = (\gamma - 1)(E - \frac{1}{2}\rho u^2)$ is the pressure. The parameter γ is a constant greater than one and equal to the ratio of the specific heats of the gas. For this equation of state we have

$$\frac{dp}{d\rho} = \frac{\gamma p}{\rho} = c^2 > 0,$$

where c is the local sound speed of the gas and is related to the characteristic velocities u, $u+c$, and $u-c$ of Eq. (1.1).

The quantities needed for Roe's scheme in (2.13) and (2.14) are derived for the Euler equations in Appendix B.

We will present numerical results for two typical Riemann problems for air ($\gamma = 1.4$) that have appeared in the literature as standard tests. The first example was used by Sod [14] to compare many of the popular numerical methods. The initial discontinuity in this problem breaks into a weak shock wave followed by a contact discontinuity and a rarefaction wave. All the variables are discontinuous across a shock wave; however, across a contact discontinuity the density is discontinuous but the pressure and velocity are continuous. In the rarefaction wave all the variables are continuous.

In the second example, suggested by P. Lax [1, 5], the initial discontinuity breaks into a moderately strong shock followed by a density level far above its initial state. The contact discontinuity then lowers the density, which is rebuilt slowly by a rarefaction wave.

In the self-adjusting grid methods, the mesh at the ξ break points is advanced on each time step according to Eq. (3.6). We experiment with the mesh velocity $\dot{\xi}_{j+1/2} = \dot{\xi}(v_j, v_{j+1})$ defined by averaging the characteristic speeds with respect to the relative jumps in the characteristic variables, according to either Eq. (3.9) or Eq. (3.13). After advancing ξ, the grid is regularized by using the procedure described in Section III.

The Riemann problem solved here can be considered an interaction problem at $t = 0$ because the initial data break into three strong waves. The mesh velocity equations were developed to be accurate for isolated waves and to give the most weight to the strongest wave by averaging during an interaction. The mesh adjustment technique can help in interactions, but there will be a loss of information depending upon the scheme's ability to resolve different waves. A procedure that may help overcome some of the scheme's difficulties is to locally refine the mesh near an interaction until the waves have separated sufficiently to be accurately resolved on the coarser reference mesh.

To test the performance of the self-adjusting mesh algorithm, the initial conditions at time t_{init} will be given both during an interaction ($t_{\text{init}} = 0$) and after the waves have separated ($t_{\text{init}} > 0$).

Both the Godunov and Roe methods compute integral values of the solution (2.1b) at x_j. In the rarefaction wave these integral values may differ significantly from the pointwise values needed by the plotting algorithm. For this reason we will plot the approximate pointwise pointwise values at $\xi_{j+1/2}$ as

$$v_{j+1/2} \equiv [(\xi_{j+1/2} - x_j)v_{j+1} + (x_{j+1} - \xi_{j+1/2})v_j]/(x_{j+1} - x_j) \tag{4.2}$$

when appropriate. The difference between these two methods will be illustrated for the Sod example.

The pointwise values of an exact solution at the mesh points will be plotted as a dashed line and the numerical solutions as a solid line. In some of the figures the numerical values of the computed solution will be designated by $\times$.

A. *The Sod Example*

In the Sod example the solution at $t = 0$ is defined by

$$\begin{array}{lcc} & 0 \leqslant x \leqslant \frac{1}{2} & \frac{1}{2} < x \leqslant 1 \\ \rho = & 1.0 & 0.125 \\ m = & 0.0 & 0.000 \\ E = & 2.5 & 0.250 \end{array} \tag{4.3}$$

The numerical calculations are shown at $t = 0.25$. All used 50 mesh points, and the CFL condition number was 0.5.

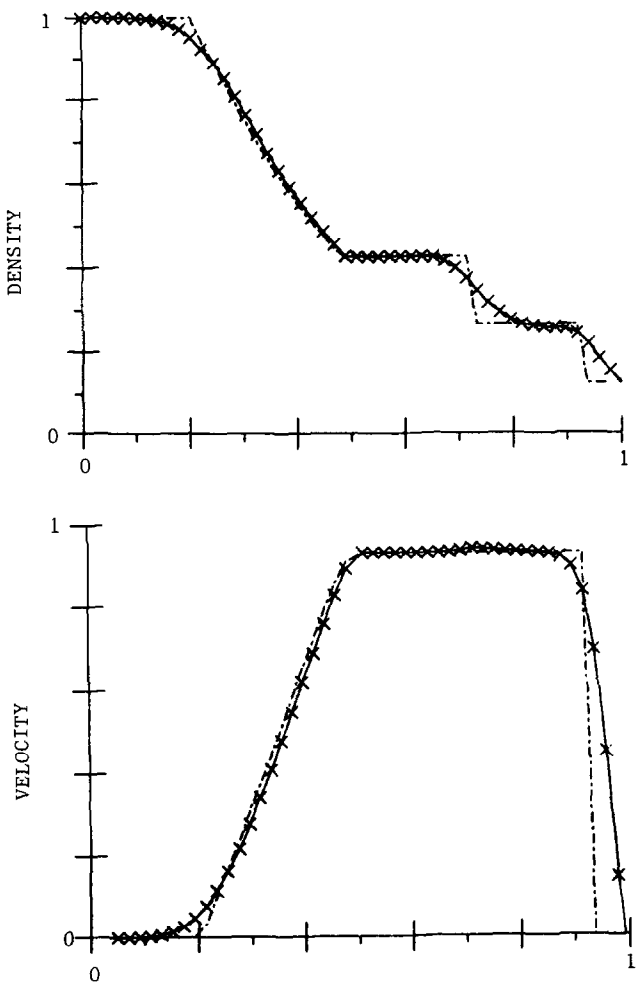

FIG. 4. The fixed grid Godunov solution to Sod's problem at $t = 0.25$ with $t_{\text{init}} = 0.125$.

We first describe the numerical results obtained when the initial conditions are taken after the waves have separated. Next we describe those results for the Riemann problem.

1. *Initial Conditions at* $t = 0.125$

The Godunov and Roe methods' results on a fixed msh are almost identical (see Figs. 4 and 5). Recall, however, that Roe's method is computationally simpler and more efficient than Godunov's. For this calculation there seems to be no advantage to using the costly exact Riemann solver over the approximate solution method. Both methods are equally bad and the shock wave and contact discontinuity are smeared almost beyond recognition.

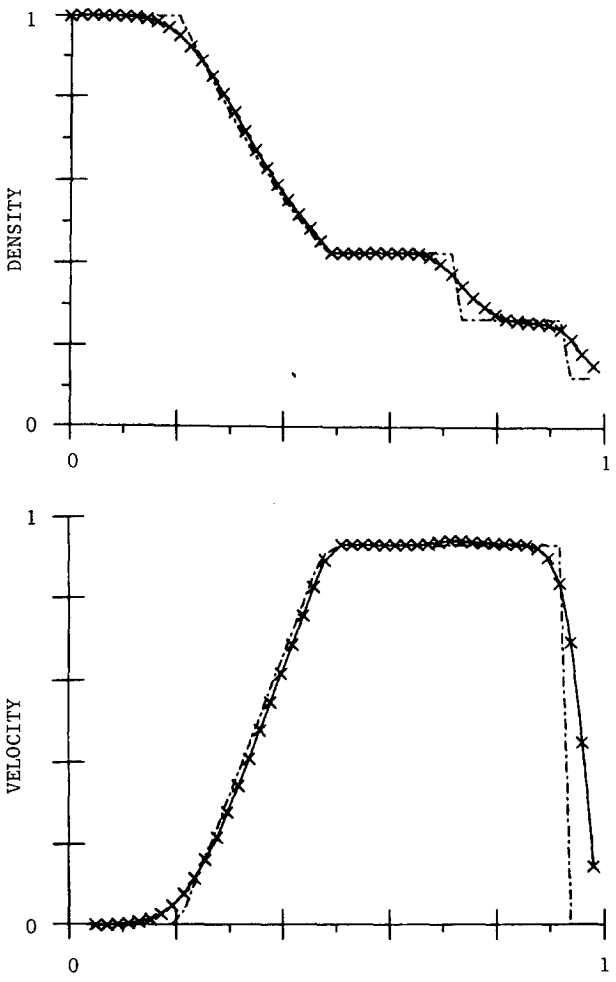

FIG. 5. The fixed grid Roe solution to Sod's problem at $t = 0.25$ with $t_{\text{init}} = 0.125$.

The only change in the algorithm used to produce the Godunov results in Fig. 6 compared to Fig. 4 is that the mesh was adjusted using Eq. (3.13) instead of being fixed. In Fig. 7 the integral values for the solution are plotted as if they were pointwise values instead of averaged according to Eq. (4.2). The mesh was adjusted according to Eq. (3.9) and Roe's method was used in Fig. 8. Note the dramatic increase in accuracy for both Godunov's and Roe's method on the self-adjusting grid. The shock wave and contact discontinuity both have been maintained to one zone. Note again how similar the Godunov and Roe method results are.

The integral values in the rarefaction wave (Fig. 7) have some imperfections (multiple constant states). These are caused by the sampling algorithm and the low-

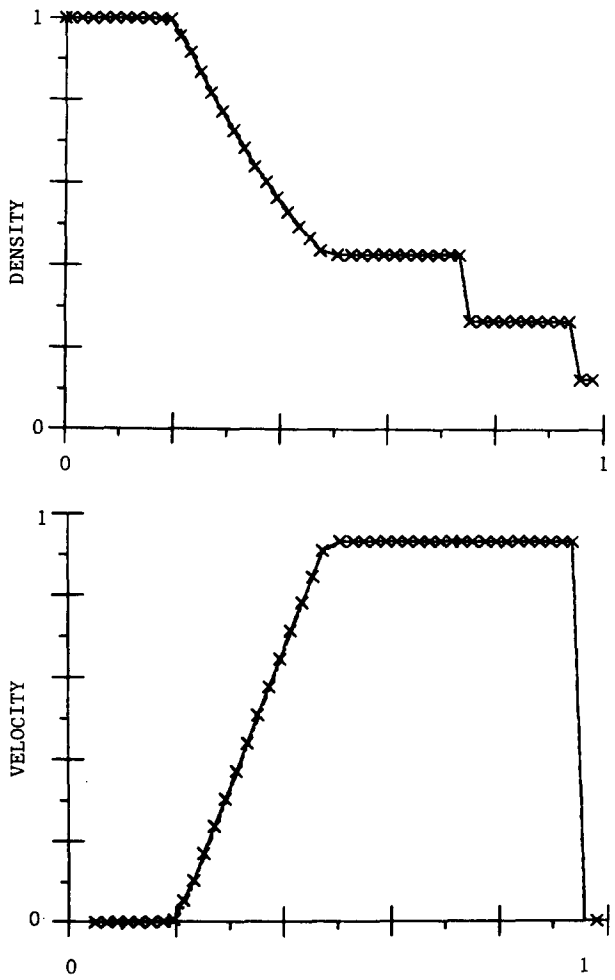

FIG. 6. The self-adjusting grid (3.13) Godunov solution to Sod's problem at $t = 0.25$ with $t_{init} = 0.125$.

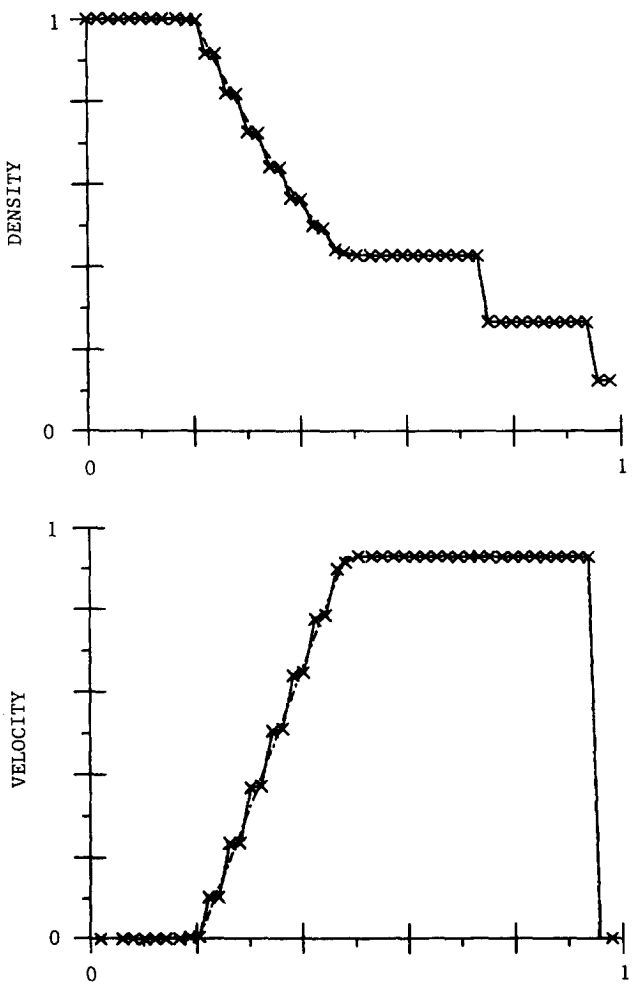

FIG. 7. Integral values of the solution in Fig. 6.

order constant state assumption used by the method much in the same way they occur in the random choice algorithm [2].

2. *Initial Condition at* $t = 0.0$

When the initial conditions are defined at $t = 0$ (the Riemann problem) by $t = 0.25$, the Godunov solution on a fixed mesh, shown in Fig. 9, has diffused even more than in Fig. 5. Again, the Roe solution (not shown) is almost indistinguishable.

Errors in the self-adjusting mesh methods (see Fig. 10) are introduced by inaccurately resolving the interactions at $t = 0$. Some of these errors are the result of averaging caused by using a low-order scheme that assumes a constant state between

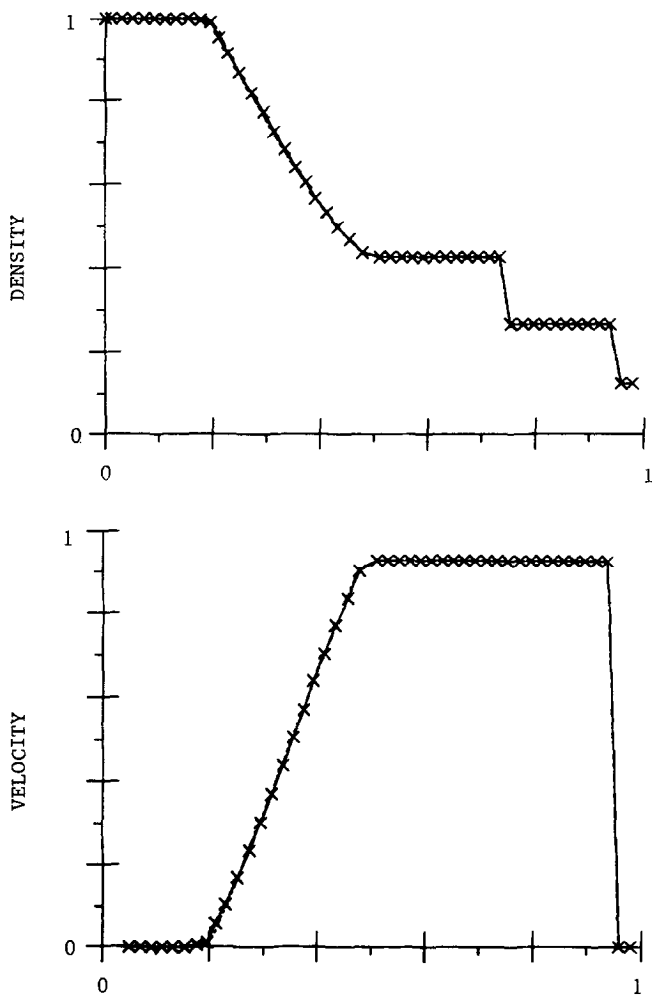

FIG. 8. The self-adjusting grid (3.9) Roe solution to Sod's problem at $t = 0.25$ with $t_{\text{init}} = 0.125$.

the ξ_l. These errors can be reduced by refining the grid around the interaction until the waves are sufficiently separated on the coarser reference grid.

Some major differences between the self-adjusting mesh methods and the fixed grid methods are

(i) the shock waves contract to one zone and maintain this resolution throughout the calculation,

(ii) errors introduced into the contact discontinuity neither grow nor shrink in time because they are an allowed solution to Eq. (1.1),

(iii) the rarefaction wave is not, in general, as smooth as is the fixed mesh calculations because the self-adjusting grid introduces far less artificial dissipation; it

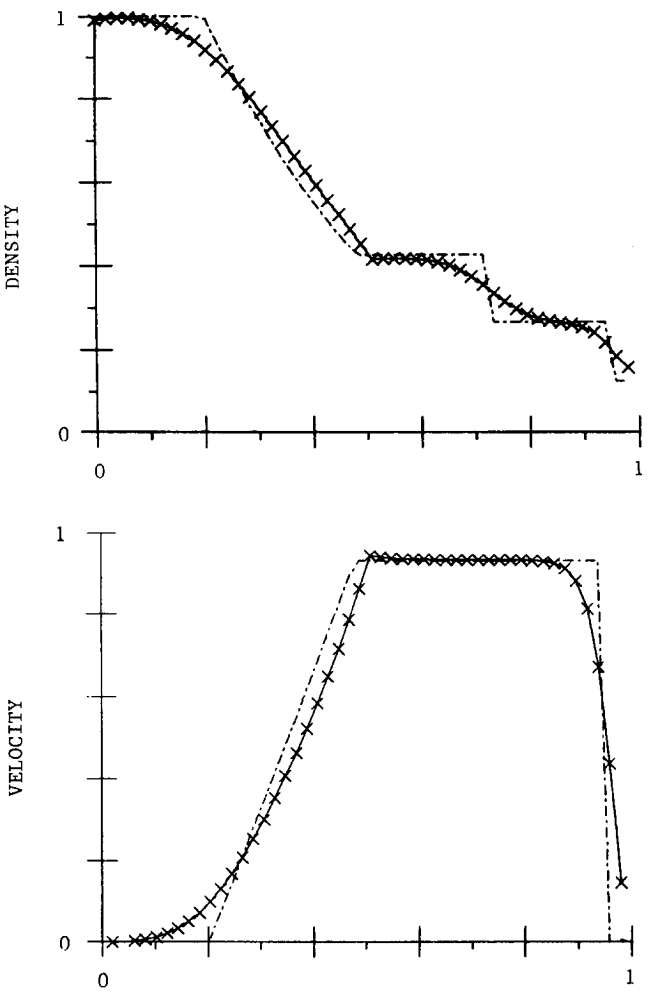

FIG. 9. The fixed grid Godunov solution to Sod's problem at $t = 0.25$ with $t_{\text{init}} = 0$.

is, however, closer to the exact solution and retains more information on the solution structure.

The Roe scheme with the entropy viscosity term was also run for this problem and no discernible differences were found between these and Fig. 10. Roe's scheme may violate entropy inequality (1.4b) unless a term such as Eq. (2.14) is used [8]. The solution shown in Fig. 11 was computed without an additional entropy viscosity term and illustrates how important the entropy viscosity is to prevent nonphysical solutions from occurring.

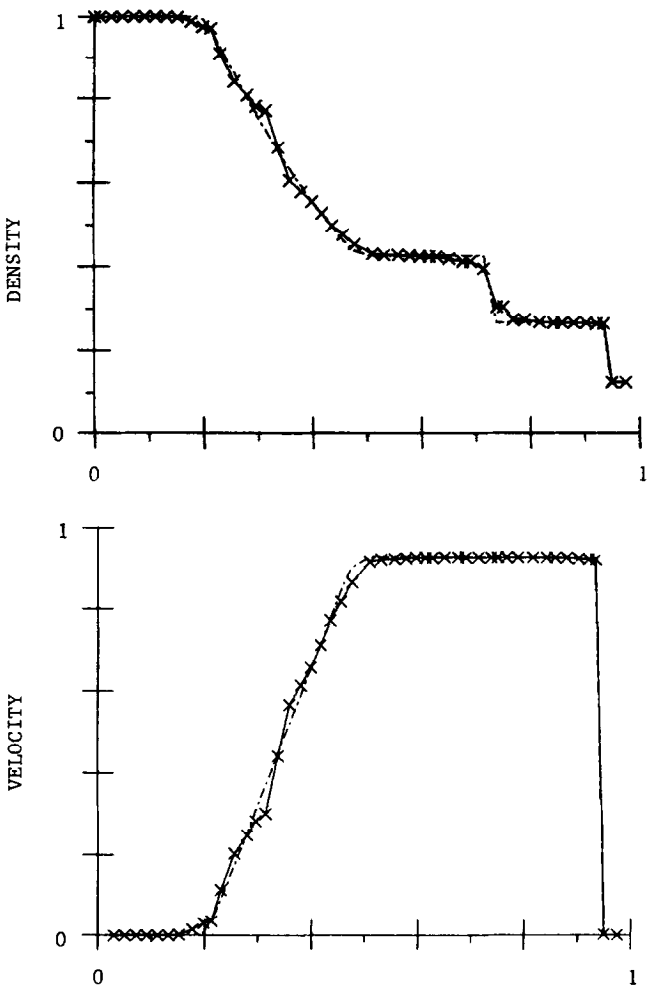

FIG. 10. The self-adjusting grid (3.13) Godunov solution to Sod's problem at $t = 0.25$ with $t_{init} = 0$.

B. *The Lax Example*

In the Lax example the solution at $t = 0$ is defined by

$$\begin{array}{lcc} & 0 \leqslant x \leqslant \frac{1}{2} & \frac{1}{2} < x \leqslant 1 \\ \rho = & 0.445 & 0.5 \\ m = & 0.311 & 0.0 \\ E = & 8.928 & 1.4275 \end{array} \tag{4.4}$$

The numerical calculations are shown at $t = 0.15$; all used 100 mesh points, and the CFL condition number was 0.5. As in the Sod example, we will first describe the

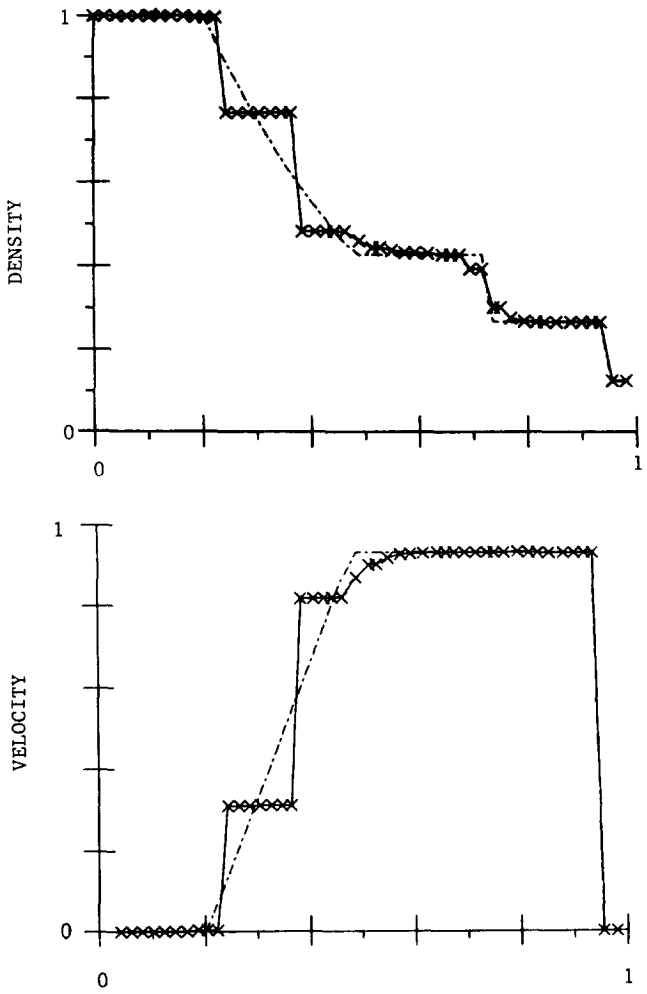

FIG. 11. The self-adjusting grid (3.9) Roe solution to Sod's problem at $t = 0.25$ with $t_{init} = 0$ and *no* entropy viscosity (2.14).

numerical results obained when the initial conditions are given after the waves have separated.

1. *Initial Conditions at* $t = 0.075$

The fixed grid solution calculated by the Godunov method is shown in Fig. 12. Even though the correct density behind the shock was given by the initial conditions, the artificial viscosity inherent in the Godunov method has reduced it to well below its correct value. Also, note the nonphysical error in the velocity and pressure profiles at the contact discontinuity location. There errors were unexpected because of the

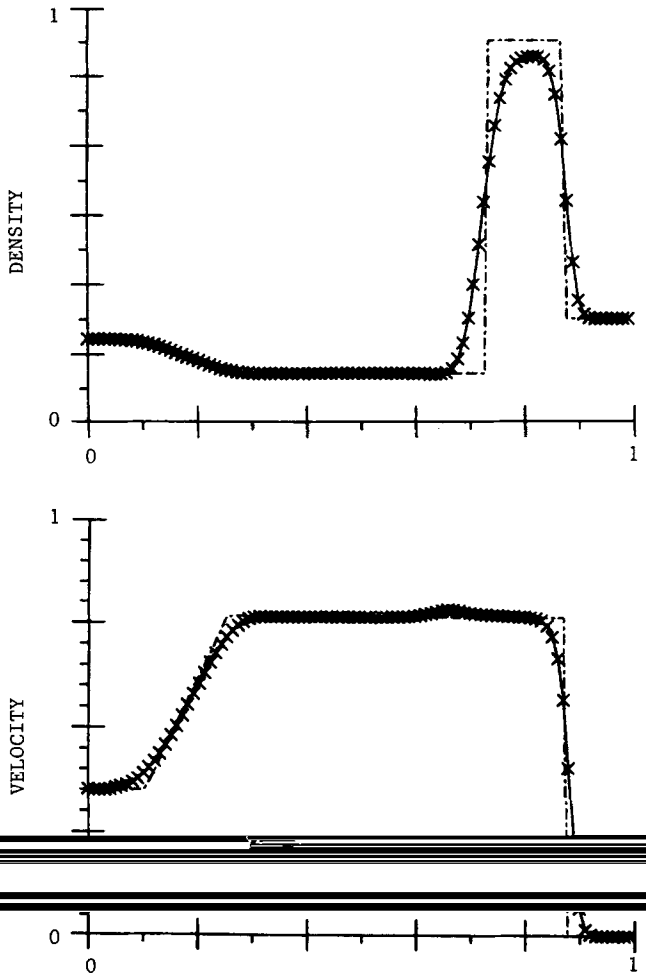

FIG. 12. The fixed grid Godunov solution to Lax's problem at $t = 0.15$ with $t_{init} = 0.075$.

monotonicity preserving properties of the method. However, these monotonicity properties are valid only for the conserved variables, not for those quantities derived from them, such as the velocity and pressure.

When self-adjusting grid algorithm (3.13) is used, the Godunov results improve considerably (see Fig. 13). The shock and contact discontinuities both have been maintained to one zero. This again demonstrates that after the waves have separated the self-adjusting mesh allows them to be tracked with little or no loss in resolution.

2. *Initial Conditions at* $t = 0$

When initial conditions (4.4) are given at $t = 0$, the fixed grid Godunov solution in Fig. 14 again exhibits the extremely diffusive nature of the scheme. Note how much

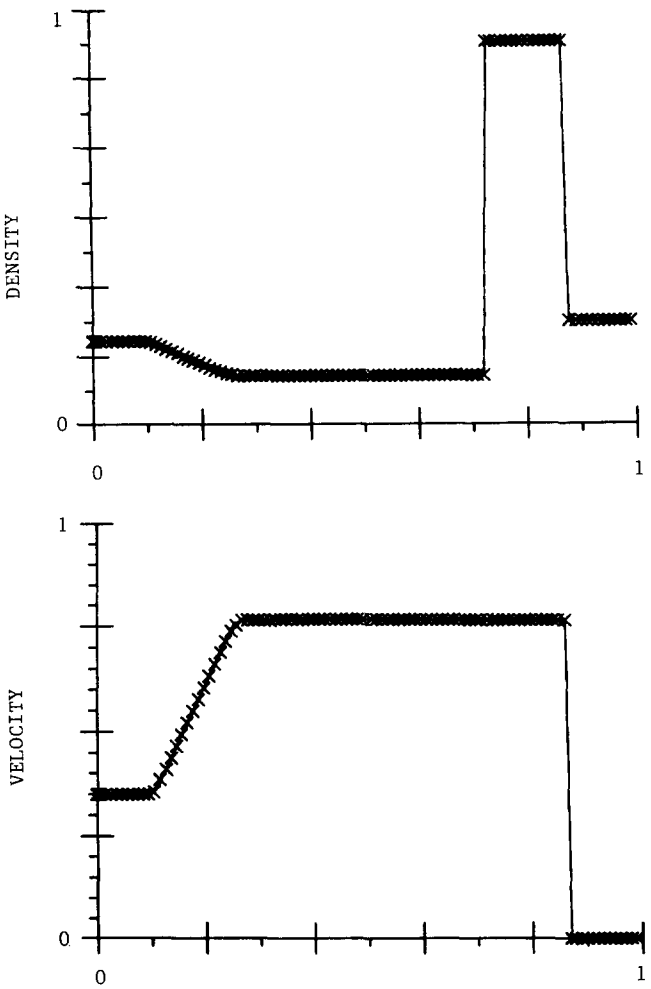

FIG. 13. The self-adjusting grid (3.13) Godunov solution to Lax's problem at $t = 0.15$ with $t_{\text{init}} = 0.075$.

the calculated rarefaction wave and the strength of the shock are in error when compared to the exact solution. These errors are due almost entirely to this overwhelming diffusion.

The self-adjusting mesh Godunov solution in Fig. 15 is much better than the fixed grid solution. The shock has compressed to one zone but the contact is not as sharp. The errors introduced into the contact during the interaction at $t = 0$ neither grow nor decay in time. The rarefaction wave is much more accurately approximated than it was in the fixed mesh calculation but is not as smooth. This difference again illustrates how much the artificial viscosity introduced by the method is reduced on a moving mesh.

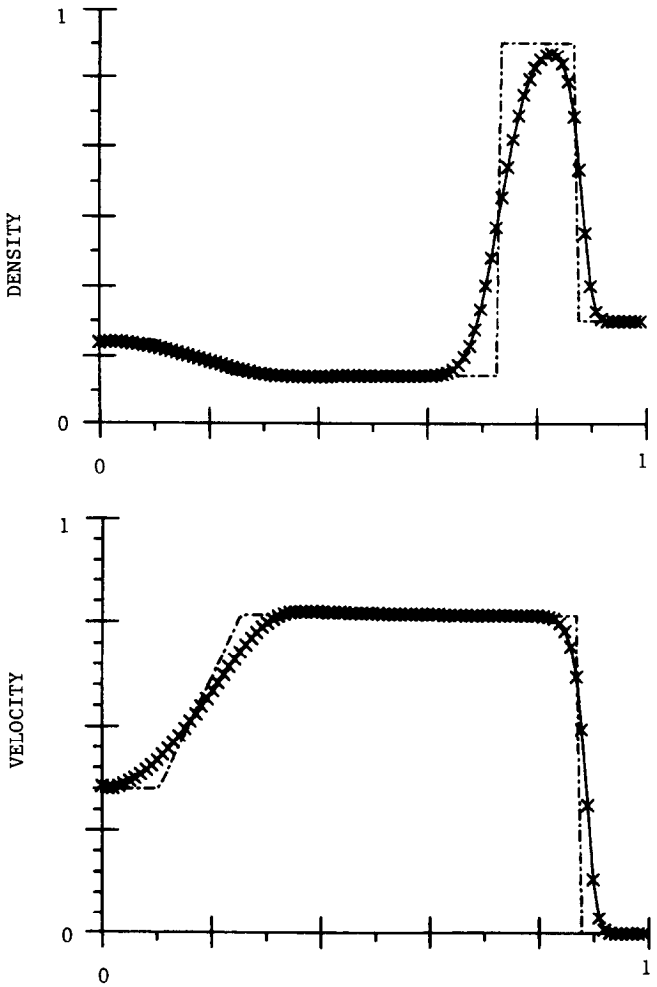

FIG. 14. The fixed grid Godunov solution to Lax's problem at $t = 0.15$ with $t_{\text{init}} = 0$.

In numerical experiments, not presented here, we found little difference between the accuracy in the solutions generated by the two different mesh velocity algorithms (3.13) and (3.9) for Roe's method. Also, we found that even though the fixed mesh algorithms are highly sensitive to the CFL number, the self-adaptive grid solutions are insensitive to changes in the CFL number between 0.1 and 0.95.

V. CONCLUSIONS

These conclusions are based on a large number of our numerical experiments, only a sample of which is presented in this report.

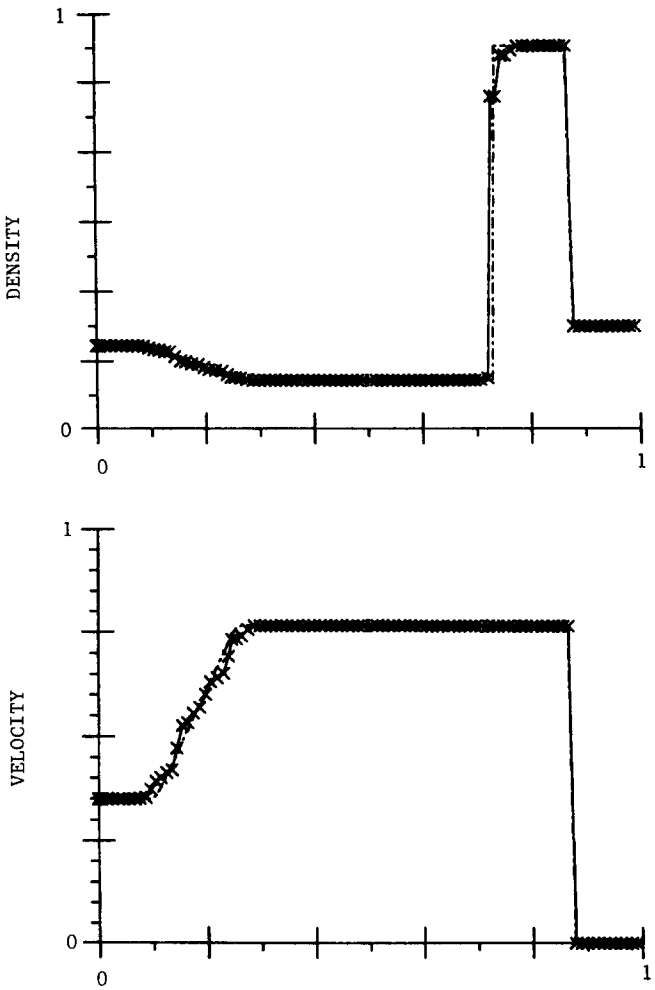

FIG. 15. The self-adjusting grid (3.13) Godunov solution to Lax's problem at $t = 0.15$ with $t_{\text{init}} = 0.0$.

First, we want to comment on the performance of the first-order Godunov-type schemes considered here and in particular to compare Roe's scheme with Godunov's scheme. Both schemes are based on a piecewise-constant approximation, the discontinuities of which are propagated as waves in a Riemann problem. We find that these schemes, as expected, handle wave propagation accurately. However, averaging is the only mechanism to simulate variations in the structure of the solution. This crude approach requires a large number of mesh points and consequently a large number of time steps to obtain a good resolution. These schemes all performed poorly in rarefaction regions and even more poorly in resolving interactions.

We found very little difference between Roe's scheme (as modified in (2.14)) and Godunov's scheme on the static or the self-adjusting grid. In fact, in most cases the results are almost identical. This finding indicates that the averaging error in the numerical method is much larger than the differences in approximating the solution to the Riemann problem.

We were surprised to find instances, as in Fig. 4, in which these Godunov-type schemes produced noticeable nonphysical oscillations in the numerical solution.

On a fixed mesh both schemes exhibit a strong dependence on the CFL number. The CFL restriction of the linear stability analysis was found adequate on both the fixed and the self-adjusting meshes. We find that the self-adjusting mesh algorithm makes the performance of the Godunov-type schemes almost independent of the CFL number.

The self-adjusting mesh algorithm reduces the diffusion caused by averaging and makes it possible for admissible discontinuities to be propagated as perfect discontinuities. Initially smeared shocks become jump discontinuities; however, a smeared contact discontinuity is propagated as such because it is an exact solution of the partial differential equation, but no further smearing occurs. Because rarefaction waves are less diffused, their description contains more information. Eliminating much of the diffusion error enables us to examine the rate at which information of spatial variation is fed into the numerical solution; we grade both methods as poor.

After removing the averaging diffusion from Roe's scheme on a self-adaptive mesh, we find that this scheme selects a negative shock rather than an expansion wave as shown in Fig. 11. The addition of the entropy viscosity developed in Appendix A remedies this. However, entropy viscosity is of order $O(\Delta x^3)$, which is enough to exclude nonphysical solution in the limit but is not enough to considerably improve the slow rate at which the rarefaction wave develops.

The underlying mesh $\{x_j\}$ need not be uniform and, in fact, may and should be adjusted periodically to the structure of the evolving solution. We feel that the number of points per unit length should be proportional to the deviation of the local Riemann problem from that of a single wave. Such a criterion should improve the quality of the numerical solutions.

We expect much better results and similar improvement in performance when applying this self-adjusting mesh algorithm to second-order accurate Godunov-like schemes (Harten and Hyman, 1982). Also, the simplicity of the self-adjusting mesh algorithm and the fact that it is free from topological and smoothness constraints should facilitate construction of a relatively simple generalization for multidimensional problems.

APPENDIX A: Entropy Viscosity for Roe's Scheme in a Moving Mesh

In this Appendix we modify the numerical flux (2.13) of Roe's scheme to include entropy considerations.

Roe's scheme is a Godunov-type scheme derived from $w(x/t; w_L, w_R)$, which is the solution to the linear Riemann problem

$$\begin{aligned} w_t + A(w_L, w_R)w_x = 0, \qquad w(x,0) &= w_L, \qquad x > 0, \\ &= w_R, \qquad x > 0, \end{aligned} \tag{A.1a}$$

where $A(w_L, w_R)$ satisfies the relation

$$f(w_R) - f(w_L) = A(w_L, w_R)(w_R - w_L). \tag{A.1b}$$

Let

$$R(w_L, w_R) = (R_1, \ldots, R_m) \tag{A.2a}$$

be a matrix, with the columns the right eigenvectors of $A(w_L, w_R)$. Hence,

$$R^{-1}A(w_L, w_R)R = D(w_L, w_R), \tag{A.2b}$$

where D is the diagonal matrix $D_{ij} = a_i \delta_{ij}$. Denote by u the vector of characteristic variables

$$w = Ru. \tag{A.3a}$$

Under transformation (A.3a), the Riemann problem (A.1a) decouples into m scalar Riemann problems for the characteristic variables

$$\begin{aligned} \frac{\partial}{\partial t} u_k + a_R(w_L, w_R)\frac{\partial}{\partial x} u_k = 0, \qquad u_k(x,0) &= u_k^L, \qquad x < 0, \\ &= u_k^R, \qquad x > 0, \end{aligned} \tag{A.3b}$$

the solution to which is

$$\begin{aligned} u_k(x/t: u_k^L, u_k^R) &= u_k^L, \qquad x/t < a_k, \\ &= u_k^R, \qquad x/t > a_k. \end{aligned} \tag{A.3c}$$

Thus, each k-wave in the Riemann problem (2.2) is approximated by a jump discontinuity of the size

$$a_k = u_k^R - u_k^L \tag{A.4}$$

that propagates with a speed a_k. This is a reasonable approximation when the k-wave is a shock or a contact discontinuity. When the k-wave is a rarefaction, its approximation by a jump discontinuity brings about entropy condition violations.

To rectify this problem we modify approximation (A.3c) by introducing an intermediate state u_k^* that simulates the diffusion introduced to a Godunov-type scheme by a continuous transition between u_k^L and u_k^R:

$$\begin{aligned} u_k(x/t; u_k^L, u_k^R) &= u_k^L, \qquad x/t \leqslant a_k^L, \\ &= u_k^*, \qquad a_k^L < x/t \leqslant a_k^R, \\ &= u_k^R, \qquad a_k^R < x/t. \end{aligned} \tag{A.5}$$

Here

$$a_k^L = a_k - \delta_k, \qquad a_k^R = a_k + \delta_k, \qquad \delta_k \geqslant 0 \tag{A.6a}$$

are to approximate the speeds of the fan endpoints if the k-wave is a rarefaction; δ_k is to vanish if and only if the k-wave is a shock.

Once δ_k is prescribed, then u_k^* is uniquely determined by the requirement of conservation (2.6b),

$$(a_k^R - a_k^L)u_k^* = (a_k - a_k^L)u_k^L + (a_k^R + a_k)u_k^R \tag{A.6b}$$

(see Fig. A.1).

Next we evaluate the flux $\bar{f}(\dot{\xi}; w_L, w_R)$ by the following steps:

$$\begin{aligned} \int_{-\Delta}^{\dot{\xi}\tau} u_k(x/\tau; u_k^L, u_k^R)\,dx &= [(\tau\dot{\xi} + \Delta) - \tau(\dot{\xi} - a_k^L)^+]u_k^L \\ &\quad + \tau[(\dot{\xi} - a_k^L)^+ - (\dot{\xi} - a_k^R)^+]u_k^* + \tau(\dot{\xi} - a_k^R)^+ u_k^R \end{aligned} \tag{A.7a}$$

where $b^+ = \max(0, b)$.

Now we use the relation $b^+ = \frac{1}{2}(b + |b|)$ to rewrite (A.7a) as

$$\begin{aligned} &\frac{1}{\tau}\left[\int_{-\Delta}^{\dot{\xi}\tau} u_k(x/\tau; u_k^L, u_k^R)\,dx - \Delta u_k^L\right] \\ &\quad = \dot{\xi}u_k^L + \tfrac{1}{2}(\dot{\xi} - a_k)a_k + \tfrac{1}{4}[|\dot{\xi} - a_k + \delta_k| + |\dot{\xi} - a_k - \delta_k|]\,a_k, \end{aligned} \tag{A.7b}$$

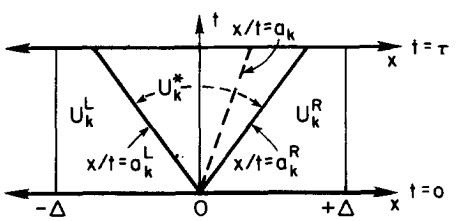

FIG. A1. Solution to the approximate Riemann problem for u_k.

where we have made use of (A.4) and (A.6). Next we use the relation

$$\frac{1}{\tau}\left[\int_{-\Delta}^{\dot{\xi}\tau} w(x/\tau; w_L, w_R)\,dx - \Delta w_L\right] = \sum_{k=1}^{m} R_k \left[\int_{-\Delta}^{\tau\dot{\xi}} u_k(x/\tau; u_k^L, u_k^R)\,dx - \Delta u_k^L\right]$$

$$k=1$$

Here $Q^k(x)$ denotes

$$\begin{aligned} Q^k(x) = \tfrac{1}{2}[|x+\delta_k| + |x-\delta_k|] &= |x|, \qquad |x| \geqslant \delta_k, \\ &= \delta_k, \qquad |x| \leqslant \delta_k. \end{aligned} \tag{A.8b}$$

Expression (2.14) for the numerical flux $\tilde{f}(\dot{\xi}; w_L, w_R)$ follows immediately from Eqs. (2.7a) and (A.8).

We turn now to describe our choice of δ_k in (A.5) and (A.8). By the Harten–Lax theorem on Godunov-type schemes (see Section II), entropy consistency of the scheme follows from that of the Riemann solver. Hence, to ensure entropy consistency of modified Roe scheme (2.14) it is sufficient to choose δ_k so that the Riemann solver (A.5) satisfies entropy inequality (2.6c).

First, let us consider the scalar case ($m = 1$), where (A.5)–(A.6) become

$$\begin{aligned} w(x/t; w_L, w_R) &= w_L, \qquad x/t < a^L, \\ &= w_*, \qquad a^L < x/t < a^R, \\ &= w_R, \qquad a^R < x/t, \end{aligned} \tag{A.9a}$$

$$(a^R - a^L) w_* = [a(w_L, w_R) - a(w_L)]\, w_L + [a(w_R) - a(w_L, w_R)]\, w_R, \tag{A.9b}$$

$$a^L = a(w_L, w_R) - \delta, \qquad a^R = a(w_L, w_R) + \delta, \tag{A.9c}$$

and

$$a(w_L, w_R)(w_R - w_L) = f(w_R) - f(w_L). \tag{A.9d}$$

Motivated by Oleinik's entropy condition we choose

$$\delta = \max_{0<\theta<1} [0, a(w_L, w_R) - a(w_L, w(\theta), a(w(\theta), w_R) - a(w_L, w_R)], \tag{A.10a}$$

where $w(\theta) = w_L + \theta(w_R - w_L)$; if $f(w)$ is convex, then it is enough to check the endpoints $\theta = 0$ and $\theta = 1$ in (A.10a); that is,

$$\delta = \max[0, a(w_L, w_R) - a(w_L), a(w_R) - a(w_L, w_R)]. \tag{A.10b}$$

Note that $\delta = 0$ if and only if the solution of the Riemann problem is a shock.

Now we show that this choice of δ implies that Riemann solver (A.9) is consistent with entropy inequality (2.6c).

Let $w_E(x/t; w_L, w_R)$ denote the exact solution of the Riemann problem. Since δ in (A.10) was chosen so that

$$w_E(y; w_L, w_R) = w(y; w_L, w_R) = w_L \qquad \text{for} \quad y < a^L$$

and

$$w_E(y; w_L, w_R) = w(y; w_L, w_R) = w_R \qquad \text{for} \quad y > a^R,$$

hence by conservation

$$(a^R - a^L) w_* = \int_{a^L}^{a^R} w_E(y; w_L, w_R)\, dy; \tag{A.11a}$$

therefore it follows from Jenssen's inequality that

$$(a^R - a^L)\, u(w_*) \leqslant \int_{a^L}^{a^R} u(w_E(y; w_L, w_R))\, dy \tag{A.11b}$$

and consequently

$$\begin{aligned} \int_{-\Delta}^{\Delta} u(w(x/t; w_L, w_R)) &\leqslant \int_{-\Delta}^{\Delta} u(w_E(y; w_L, w_R))\, dy \\ &\leqslant \Delta[u(w_L) + u(w_R)] - \tau[F(w_R) - F(w_L)]. \end{aligned} \tag{A.11c}$$

The last inequality follows from the fact that the exact solution satisfies (2.6c). This completes the proof that modified Roe scheme (2.14) with (A.10) satisfies the entropy condition in the scalar case.

Numerical experiments described in Section IV support the conjecture that modified Roe scheme (2.14) with (A.12) is consistent with the entropy inequality also in the system case.

Remark. It is interesting to note that if the average state u_R^* in (A.5) is replaced by a linear transition $u_k^*(x/t)$, where

$$u_k^*(y) = u_k^L + \frac{y - a_k^L}{a_k^R - a_k^L}(u_k^R - u_k^L) \qquad \text{for} \quad a_k^L < y < a_k^R,$$

then the resulting scheme is (2.14) with $Q_k^*(x)$ defined by

$$Q_k^*(x) = |x|, \qquad \text{for} \quad |x| \geqslant \delta_k,$$
$$= \tfrac{1}{2}((x^2/\delta_k) + \delta_k), \qquad \text{for} \quad |x| \leqslant \delta_k.$$

This function is a continuously differentiable approximation to $|x|$.

Next we describe the choice of δ_k in the case of systems of conservation laws. In the spirit of Liu's extension of Oleinik's entropy conditions to systems, we propose to apply (A.10) to each of the k-waves, i.e.,

$$\delta_k = \max_{0 \leqslant \theta \leqslant 1} [0, a_k(w_L, w_R) - a_k(w_L, w(\theta)), a_k(w(\theta), w_R) - a_k(w_L, w_R)] \tag{A.12a}$$

and in the case of a convex equation of state

$$\delta_k = \max[0, a_R(w_L, w_R) - a_R(w_L), a_R(w_R) - a_R(w_L, w_R)]. \tag{A.12b}$$

Let us now consider a Riemann problem where w_L and w_R satisfy RH relation (1.4a) with some speed of propagation S. It follows from (2.12a) that $w_R - w_L = \alpha_R R_R(w_L, w_R)$ and $S = a_R(w_L, w_R)$ for some $k = k_0$. Hence our approximate Riemann solver is just (A.9) with (A.12) for $k = k_0$. In this case we can use the exact same argument of the scalar case and conclude by (A.11) that the Riemann solver satisfies entropy inequality (2.6c).

On the other hand, the modified Roe scheme is in conservation form; therefore, its limit solution is a weak solution of (1.1). Hence, the only entropy violation possible in the limit solution is that of an "expansion shock," i.e., a discontinuity which satisfies RH condition (1.4a) but not entropy inequality (1.4b); this is exactly the case considered above.

APPENDIX B: ROE'S SCHEME FOR ONE-DIMENSIONAL EULER EQUATIONS

In this Appendix we describe how to compute the quantities a_k, R_k, and α_k in Roe's scheme (2.12)–(2.14) for the Euler equations of gas dynamics (4.1). Define

$$\bar{u} = \langle \rho^{1/2} u \rangle / \langle \rho^{1/2} \rangle, \tag{B.1a}$$

$$\bar{h} = \langle \rho^{1/2} h \rangle / \langle \rho^{1/2} \rangle, \tag{B.1b}$$

and

$$\bar{c} = [(\gamma - 1)(\bar{h} - \tfrac{1}{2}\bar{u}^2)]^{1/2}, \tag{B.1c}$$

where $h = (E + p)/\rho$ is the enthalpy and $\langle w \rangle$ denotes

$$\langle w \rangle = \tfrac{1}{2}(w_L + w_R). \tag{B.1d}$$

Then the eigenvalues of (2.12a) are

$$a_1(w_L, w_R) = \bar{u} - \bar{c}; \qquad a_2(w_L, w_R) = \bar{u}; \qquad a_3(w_L, w_R) = \bar{u} + \bar{c}; \tag{B.2}$$

and the corresponding eigenvectors are

$$R_1 = \begin{pmatrix} 1 \\ \bar{u} - \bar{c} \\ \bar{h} - \bar{u}\bar{c} \end{pmatrix}; \qquad R_2 = \begin{pmatrix} 1 \\ \bar{u} \\ \tfrac{1}{2}\bar{u}^2 \end{pmatrix}; \qquad R_3 = \begin{pmatrix} 1 \\ \bar{u} + \bar{c} \\ \bar{h} + \bar{u}\bar{c} \end{pmatrix}. \tag{B.3}$$

To obtain expressions for $\alpha_1(w_L, w_R)$, $\alpha_2(w_L, w_R)$, $\alpha_3(w_L, w_R)$ in (2.13b), define

$$c_1 = (\gamma - 1)([E_R - E_L] + \tfrac{1}{2}\bar{u}^2[\rho_R - \rho_L] - \bar{u}[m_R - m_L])/\bar{c}^2 \tag{B.4a}$$

and

$$c_2 = ([m_R - m_L] - \bar{u}[\rho_R - \rho_L])/\bar{c}, \tag{B.4b}$$

then evaluate α_1, α_2, α_3 by

$$\alpha_1 = \tfrac{1}{2}(c_1 - c_2), \tag{B.5a}$$

$$\alpha_2 = [\rho_R - \rho_L] - c_1, \tag{B.5b}$$

and

$$\alpha_3 = \tfrac{1}{2}(c_1 + c_2). \tag{B.5c}$$

REFERENCES

1. S. Z. BURSTEIN, *J. Comput. Phys.* **1** (1966), 198.
2. A. J. CHORIN, *J. Comput. Phys.* **22** (1976), 517.
3. S. K. GODUNOV, *Mat. Sb.* **47** (1959), 271.
4. A. HARTEN, "On the Symmetric Form of Systems of Conservation Laws with Entropy," Institute for Computer Applications in Science and Engineering Report No. 81-34, 1981.
5. A. HARTEN, *Math. Comput.* **32** (1978), 363.
6. A. HARTEN AND J. M. HYMAN, "Second-Order Self-Adaptive Grid Methods for One-Dimensional Hyperbolic Conservation Laws," Los Alamos National Laboratory, Los Alamos, N. Mex., 1982, in preparation.
7. A. HARTEN AND P. D. LAX, *SIAM J. Numer. Anal.* **18** (2) (1981), 289.
8. A. HARTEN, P. D. LAX, AND B. VAN LEER, "On Upstream Differencing and Godunov-Type Schemes for Hyperbolic Conservation Laws," ICASE Report, 1982; *SIAM Rev.*, to appear.
9. J. M. HYMAN, "Adaptive Mesh Strategies for the Numerical Solution of Differential Equations," Los Alamos National Laboratory Preprint LA-UR-81-2594, Los Alamos, N. Mex., 1981.

10. P. D. LAX, "Hyperbolic Systems of Conservation Laws and the Mathematical Theory of Shock Waves," SIAM, Philadelphia, Pa., 1972.
11. R. D. RICHTMYER AND K. W. MORTON, "Difference Methods for Initial-Value Problems," Interscience, New York, 1967.
12. P. L. ROE, *in* "Proceedings, Seventh International Conference on Numerical Methods in Fluid Dynamics" (W. C. Reynolds and R. W. MacCormack, Eds.), pp. 354–359, Springer-Verlag, New York, 1981.
13. P. L. ROE, *J. Comput. Phys.* **43** (1982), 357. to appear.
14. G. A. SOD, *J. Comput. Phys.* **27** (1) (1978), 1.